Large-Scale PV Plant With a Robust Controller Considering Power Oscillation Damping

Rakibuzzaman Shah, *Student Member, IEEE*, Nadarajah Mithulananthan, *Senior Member, IEEE*, and Kwang Y. Lee, *Fellow, IEEE*

***Abstract*—Transmission voltage-level photovoltaic (PV) plants are becoming reality in many developed and developing countries around the world. Studies suggest that large-scale PV plants could have either positive or negative influence on low-frequency oscillation (LFO) depending on their locations and sizes. Given the fact that these plants cannot be placed in ideal locations to minimize their impact on LFO, it is important to consider designing a damping controller for flawless integration. In this paper, a minimax linear quadratic Gaussian-based power oscillation damper (POD) for a large-scale PV plant is proposed for interarea oscillation damping. A benchmark power system prone to power system oscillations is used to demonstrate the damping performance of the designed controller considering feedback signal transmission delay. The performance of the designed controller is evaluated under different operating conditions as compared to the classical POD at PV plant. Simulation results demonstrate that the proposed controller for a PV plant provides sufficient damping to the interarea mode for a wide range of operating conditions.**

***Index Terms*—Damping controller, interarea mode, minimax linear quadratic Gaussian (LQG), uncertainties.**

I. Introduction

FOLLOWING the renewable energy regulation in Canada, U.S., China, Germany, and Australia, transmission voltage-level photovoltaic (PV) plants ranging from 10 MW to more than 250 MW are either already embedded or expected to be integrated into the existing transmission networks [1]. Majority of large-scale PVs including proposed projects are geographically far away from load centers and connected to relatively weak transmission networks. Increased PV penetrations on weak transmission link raise the concerns of possible negative impacts on power system stability as speculated by a number of studies [2]–[7]. One particular aspect is the effect of high PV penetrations on low frequency electromechanical (EM) modes, as well as on possible emergence of new lightly damped modes.

Low-frequency oscillation (LFO) stability studies advocate that, depending on penetration level, location and control techniques, large-scale PV plants could have an adverse effect on critical EM modes [4], [5]. However, due to intermittent and volatile solar insolation to the PV plant, it is recommended to have some auxiliary devices in the PV system, such as battery energy storage or ultracapacitor to meet the grid-code requirements for interconnection [6]. Recently, the impact of such auxiliary devices on oscillation damping has been assessed, and it was shown that these auxiliary devices have a positive impact on the damping of EM modes for certain operating conditions [7], [8]. But, the large-scale application of energy storage devices is still limited due to the cost of the technology. Moreover, the increased penetration of PV on power systems has imposed the requirement that PV plants should also contribute to the network support for widely varying operating conditions, necessitating design of a robust power oscillation damping loop for PV plants.

In this paper, a minimax linear quadratic Gaussian (LQG)-based power oscillation damper (POD) for a PV plant has been proposed for interarea oscillation damping. The H_∞ optimization with linear matrix inequalities has been predominantly used for a robust controller design in nonlinear systems including power system [9], [10]. However, the H_∞-based control schemes typically address the worst case scenarios and therefore too conservative when dealing with less severe disturbances and model uncertainties [10]. The minimax optimal controllers, having similar structure to that of the H_∞ controllers, also guarantee the robustness properties. Unlike H_∞ controller in which a nonconvex performance index is optimized, the minimax LQG is obtained by minimizing a convex optimization. In the minimax LQG optimal controller design, robustness is achieved via optimization of the worst case scenario of the underlying system, subject to time-domain integral quadratic constraints (IQCs) on the admissible uncertainty. The use of IQCs allows control engineers to utilize available information about the magnitude and structure of admissible uncertainties. These features of minimax optimal controllers are often very useful in achieving an acceptable tradeoff between performance and robustness [9], [11]. The effectiveness of the minimax LQG control scheme in power system has already been recognized [12]. However, the effectiveness of this control scheme for the centralized POD design in large- and multimachine power systems is yet to be seen.

The remainder of this paper is organized as follows: Section II provides the modeling overview of a large-scale PV plant including a list of the mechanisms by which PV plants could affect the EM modes. Section II also illustrates the power system modeling overview. Section III provides some mathematical background on the minimax LQG controller design as well as μ-analysis scheme. Section IV illustrates the test system

Manuscript received March 16, 2012; revised October 15, 2012; accepted November 21, 2012. Date of publication December 13, 2012; date of current version February 7, 2013. Paper no. TEC-00116-2012.

R. Shah and N. Mithulananthan are with the School of Information Technology and Electrical Engineering, The University of Queensland, Brisbane, Qld. 4072, Australia (e-mail: md.shah@uq.edu.au; mithulan@itee.uq.edu.au).

K. Y. Lee is with the Department of Electrical and Computer Engineering, Baylor University, Waco, TX 76798-7356 USA (e-mail: Kwang_Y_Lee@baylor.edu).

Color versions of one or more of the figures in this paper are available online at http://ieeexplore.ieee.org.

Digital Object Identifier 10.1109/TEC.2012.2230328

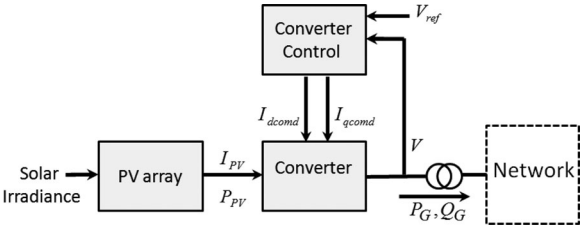

Fig. 1. Block diagram of PV with a type-4 WTG grid-side converter.

and POD design algorithm and procedure. Controller performance evaluation is presented in Section V. Finally, in Section VI, conclusions are duly drawn.

II. PV Model and Its Influence on LFO

Numerous PV generator models have been developed and used in literatures. However, a PV model based on a manufacturer-provided field or factory tests as a benchmark for stability analysis is required. Thus, in this paper, a *generic* (*standardized*) *model* of a PV plant is considered as it has been validated and widely used for power system stability analysis [13].

A. Overview of a PV Generator Model

The model of large-scale PV plants includes PV array, converter dynamics, and associated control systems. According to NERC's special report on standard models for variable generation [14], a PV model can be based on the grid-side model of the type-4 wind turbine generator (WTG) as shown in Fig. 1. From the figure, it can be seen that the power generated is processed through the power converter, which serves as a buffer between the generator and the grid and controls reactive power or voltage at the point of common coupling (PCC).

A mathematical description of current–voltage terminal characteristics of PV cells is available in the literature [15]. The single exponential function which models a PV cell is derived from the physics of the PN junction and extended to get the PV array output current as follows [15]:

$$I_{\rm PV} = I_{\rm SCA}(G) - N_p \times I_0 \left[\exp \frac{(V_A + I_{\rm PV} R_S)q}{nN_S kT} - 1\right] \quad (1)$$

where $I_{\rm PV}$ = array current (A), V_A = array voltage (V), q = charge of an electron $(1.6 \times 10^{-19}\ {\rm C})$, k = Boltzmann's constant (1.38×10^{-19}), n = ideality factor, T = temperature (K), I_0 = reverse saturation current of diode (A), R_S = array series resistance (Ω), $I_{\rm SCA}(G) = N_P I_{\rm SC}(G)$, $I_{\rm SC}$ = cell short-circuit current (A), G = solar insolation (W/m^2), N_P = number of modules in parallel; $N_S = N_{\rm CS} N_{\rm SM}$, , $N_{\rm CS}$ = number of series-connected cells in a module, and $N_{\rm SM}$ = number of modules in series.

As seen from Fig. 1, there are two main components contributing the dynamic behavior of the PV: converter and converter control. Fig. 2 depicted the block diagram of the grid-side converter and control of PV. The figure also depicted the proposed PV POD, which will be discussed later in this section. There are different possibilities for converter transfer functions; however, the following two are probably the most appropriate [16]: 1) the first-order function with unity steady-state gain; and 2) the closed-loop controller transfer function. Moreover, both provide very similar results; hence, the first one is adopted in this paper. Fig. 2 dictates that the active power to be delivered to the system is based on the solar power profile $P_{\rm PV}$, whereas reactive power generation depends on the comparative signal generated from reactive power control. Fig. 3 shows the reactive power controller of PV. The control mode can be switched to either power factor (PF) control mode or voltage control (VC) mode. Depending on the required control task, each of this control unit can be activated by proper flag. In this paper, the voltage control mode operation of a PV plant has been considered, and the reference voltage $V_{\rm ref}$ generated by the voltage control in Fig. 3 becomes a reactive power control input to the converter control in Fig. 2. The details of the model presented here can be found in [17].

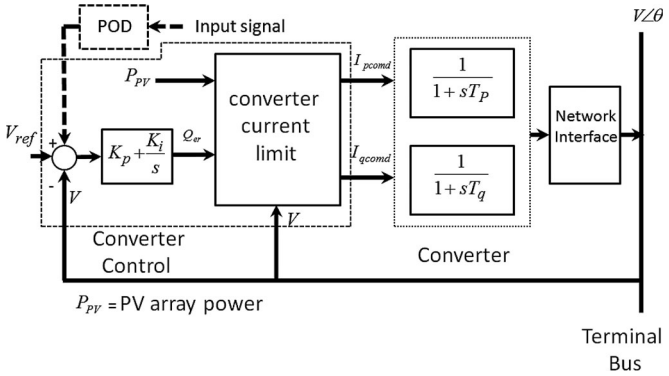

Fig. 2. Block diagram of a grid-side converter and control of PV.

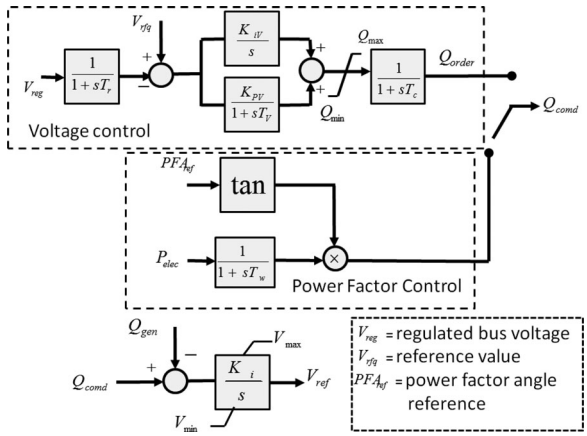

Fig. 3. Reactive power controller of PV [17].

Generally, real power modulation is used for oscillation damping. When damping control is based on real power modulation, renewable energy source normally has to curtail its real power output. Since the amount of real power that can be delivered from such sources at any time is subjected to the environmental conditions, the owner wants to deliver maximum available power. If the reactive power modulation is applied, damping of the critical mode increases with power flow through the transmission line and injected power from renewable energy

sources [18]. Hence, we have considered reactive power modulation technique in a PV plant for oscillation damping, and line power or current is considered as input to the POD.

B. Influence of Large-Scale PV on LFO

The impact of a PV plant on power system stability is minimal when deployed in small scale. However, when penetration level increases, the dynamic performance of the power system can be significantly affected [2], [3]. Since PV plants are based on power electronics converters, there are primarily four mechanisms by which the EM modes can be affected. These are as follows.

1) Redispatch of conventional generators with power system stabilizers (PSS) due to PV power.
2) By impacting on the major line flows in the system.
3) Controller interaction between PV plant controls and nearby synchronous generators.
4) The physical difference between the synchronous generators and PV generators, i.e., inertial contribution of rotating mass.

For power system with large-scale PV penetration, due to the aforementioned mechanisms, the damping of EM and other lightly damped modes can be affected negatively as reported in [4], [5], and [7]. Tuning of a PSS could help to improve the damping of EM modes. But, it requires coordinated tuning of PSSs; otherwise, a tuned PSS could have a detrimental effect on system transient stability [19]. Moreover, retuning of a PSS can be time consuming with high computational burden, which limits optimal real-time operation [20]. On the contrary, the centralized POD at a PV plant can ensure the required system performance without retuning of other system controllers. This type of a controller at the PV plant would allow a flawless integration.

C. Power System Model

A power system can be modeled at several levels of complexity, depending on the intended analytical studies of the power system. In this section, the dynamic model of a synchronous generator and its controller are illustrated to provide general framework for eigenvalue analysis and time-domain simulation, and details are summarized in Appendix A.

1) Synchronous Generator Model: Although generator modeling is rather well established, for completeness, the modeling of the generator is briefly reviewed here. Generator can be modeled with different levels of complexity depending on the intended application of the model. In this paper, the synchronous generator is modeled with the sixth-order model, which considers field winding and the damper winding. Under typical assumptions, the nonlinear equations associated with the sixth-order model of a synchronous generator are given in the appendix [21].

2) Exciter and PSS Model: In general, the integrated generator model consists of excitation system. In this paper, the simplified version of the IEEE type DC1 excitation system is used for all synchronous generators [22]. Fig. 15 in the appendix depicted the typical block diagram of the simplified IEEE type DC1 exciter. The IEEE type DC1 includes an additional lead–lag block before the amplifier block. However, the lead–lag block is often neglected. The detail can be found in [21] and [22].

A PSS can be viewed as an additional block of a generator excitation system. The PSS uses auxiliary stabilizing signals such as shaft speed, terminal frequency, and/or power to change the input signal to the exciter. The block diagram of the PSS used in this paper is depicted in Fig. 16 in the appendix.

III. Mathematical Background

A. State-Space Representation With Time Delays

The power system model consists of a set of differential algebraic equations, which describes the nonlinear model of generators, loads, PV generators, and the associated controls. A linearized model of the power system is usually obtained by linearizing the nonlinear differential algebraic equations via Taylor series expansion around an equilibrium point. Detail of the linearization of the power system nonlinear equations around the equilibrium point can be found in [21], and the generalized form of the state-space representation of power system is as follows:

$$\Delta\dot{x} = A\Delta x + B\Delta u \tag{2}$$

$$\Delta y = C\Delta x + D\Delta u \tag{3}$$

where $\Delta x, \Delta y$, and Δu are, respectively, the system state, output and input deviations from an operating point, and A, B, C, and D are the matrices of the linearized system model. The detailed linearized representation of the power system nonlinear equations will not be included in this paper due to space limitations.

Several studies suggest that due to the lack of information in local signal for certain critical/interarea mode, damping of interarea mode using remote signal/wide-area signal is more preferred [23]. Thus, in this paper, the POD at PV is designed by using wide-area signal. Design scheme using wide-area signal presents several challenges since the time delays are involved in the transmission channel. Time delays bring about a phase lag which can affect the controller performance and interactions among system dynamics. Thereby, the time delays associated with wide-area signal transmission need to be considered in the design. Time delays are usually modeled by a first-order Padé approximation [24] with a transfer function as follows:

$$G_P = \frac{1 - \frac{Ts}{2}}{1 + \frac{Ts}{2}} \tag{4}$$

where T is the delay time.

The state-space representation of the time delay can be expressed as

$$\Delta\dot{x}_d = A_d\Delta x_d + B_d\Delta u_d \tag{5}$$

$$\Delta y_d = C_d\Delta x_d + D_d\Delta u_d \tag{6}$$

where Δx_d is the delay state vector, Δu_d delay input vector, and Δy_d is the delay output vector. The delay free system described by (2) and (3) can be connected in cascade with (5) and (6) to get the system with output time delay and can be expressed as

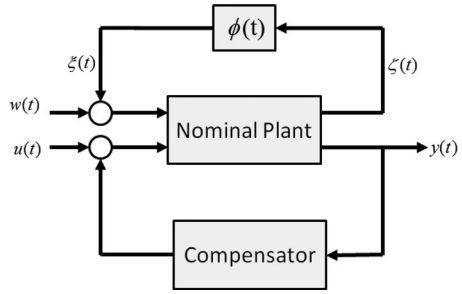

Fig. 4. Minimax LQG control scheme.

follows:

$$A_1 = \begin{bmatrix} A & 0 \\ B_d C & A_d \end{bmatrix}, B_1 = \begin{bmatrix} B \\ B_d D \end{bmatrix}$$
$$C_2 = [\, D_d C \quad C_d \,]. \tag{7}$$

Different time delays for wide-area signal transmission and their effect on overall system performance are reported in literatures [23]–[25]. Time delays are involved in signal transmission delay from measurement unit to the controller and then to control site. As the proposed POD is located at the PV generator, signal transmission delay between the controller and control site is neglected in this study. A constant time delay of 100 ms (signal transmission delay between measurement and controller) reported in [10] is used in this research for POD design.

B. Minimax LQG Control Design Preliminaries

The minimax LQG control scheme has been used in this paper for a damping controller design. The general control configuration for minimax LQG control is illustrated in Fig. 4.

To facilitate the design of a POD controller by minimax LQG, the linearized power system model need to be summarized as [11]

$$\dot{\Delta x} = A_1 \Delta x(t) + B_1 \Delta u(t) + B_2 \xi(t) + B_2 w(t) \tag{8}$$
$$\Delta y(t) = C_2 \Delta x(t) + D_2 \xi(t) + D_2 w(t) \tag{9}$$
$$\zeta(t) = C_1 \Delta x(t) \tag{10}$$

where $\zeta(t)$ is known as uncertainty output, $y(t)$ is the measured output, $w(t)$ is a unity-covariance Gaussian white noise process corresponding to the nominal disturbance, and $\xi(t)$ is an uncertainty input. The minimax LQG method for a POD design is applied to the system of the following form shown in Fig. 5.

Cost function J associated with the uncertain system (8)–(10) on infinite-time horizon can be expressed as

$$J = \lim_{T\to\infty} \frac{1}{2T} E \int_0^T (\Delta x(t)^T R \Delta x(t) + \Delta u(t)^T G \Delta u(t)) dt \tag{11}$$

where $R \geq 0$ and $G > 0, R \in R^{n\times n}, G \in R^{m\times m}$ and E are the expectation operator. The minimax optimal control finds the controller which minimizes J over all admissible uncertainties. The cost function shown in (11) can be formed in finite-time horizon. Optimal control cost function on finite horizon solution

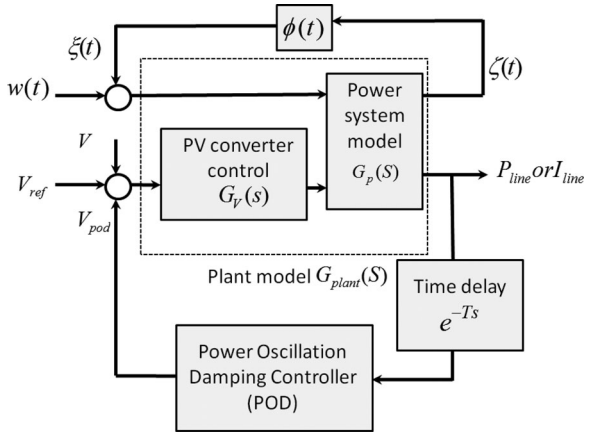

Fig. 5. Damping control design scheme for PV.

is mathematically intractable as it requires solving differential Riccati equations where the gain of the controller needs to be updated in each time steps. On the other hand, infinite horizon formulation considered time average property of the system, and it requires solving only the algebraic Riccati equations which is mathematically tractable [11]. Hence, this technique has been widely used in the controller design of complex systems including power systems [12], [26], [27]. However, in practice the infinite horizon problem can be solved in finite horizon as mentioned in [11], [28]. The details of minimax LQG control in infinite horizon are presented in Appendix B.

The step by step procedure of a minimax LQG-based POD controller design for a large-scale PV is presented in Section IV.

C. Robustness Analysis

The general approach in the design of power system damping controllers is based on the linearization of power system model around the nominal operating condition and tested on some selected operating points for controller performance evaluation. Even though this assessment procedure is simple, it does not guarantee the controller robustness as the power system continuously experience different perturbations and changes of operating conditions [29], [30]. In recent years, power system researchers have studied the application of robust control techniques to design power system controllers, even though the controller is designed by the robust technique, the robustness of the controller may not be guaranteed over a wide range of system uncertainty conditions [30]. It is, therefore, essential to rely on some effective method to evaluate the robustness of a power system controller.

Among many different techniques, the analysis using structured singular value (s.s.v.) theory is an effective method to evaluate the robustness of the power system controllers [29], [30]. The general framework of many robust control studies is based on a linear fractional transformation (LFT) described in Fig. 6. In the figure, M is a complex transfer matrix as follows:

$$M = \begin{bmatrix} M_{11} & M_{12} \\ M_{21} & M_{22} \end{bmatrix} \in C^{(p_1+p_2)\times(q_1+q_2)}. \tag{12}$$

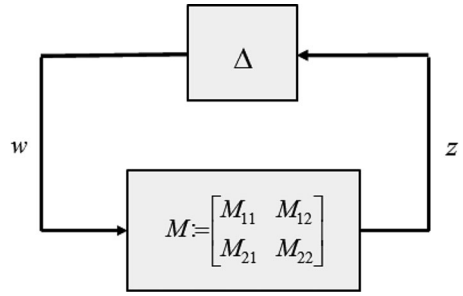

Fig. 6. Interconnection structure for robust stability analysis.

$\Delta \in C^{q_1 \times p_1}$ is another complex matrix. The upper LFT with respect to Δ is defined as

$$F_u(M, \Delta) := M_{22} + M_{21}\Delta(I - M_{11}\Delta)^{-1}M_{12} \quad (13)$$

where M_{22} represented the nominal unperturbed system, Δ is the perturbation, M_{11}, M_{12}, and M_{21} is the prior knowledge as how the perturbation affects the nominal transfer matrix. The transfer matrix Δ represents all sources of uncertainties and can be expressed as follows:

$$\Delta = \{diag[\delta_1 I_{r1}, ..., \delta_s I_{rs}, \Delta_1, ...\Delta_F]\} \quad (14)$$

where $\delta_i \in R, \Delta_j \in C^{m_j \times m_j}, \delta_i$ represents repeated scalar block, and Δ_j represents the number of full blocks.

Given the interconnection system, as depicted in Fig. 6, the s.s.v. orμ is defined as the smallest structured uncertainty Δ, measured in terms of its maximum singular value which makes $\det(I - M\Delta) = 0$:

$$\mu(M)^{-1} := \min\{\bar{\sigma}(\Delta) : \Delta \in \Delta, \det(I - M\Delta) = 0\} \quad (15)$$

where the value of $\mu(M)$ determines the allowable size of uncertainty for which the plant is robustly stable. It is shown in [29] that the system in Fig. 6 is stable for all Δ with $\|\Delta\|_\infty \leq 1$ if and only if M is stable and $\max\mu(M) < 1$.

IV. Test System and a Controller Design Procedure

A. Test System

A one-line diagram of a two-area test system is depicted in Fig. 7. This system consists of four synchronous generators associated with four 20/230-kV step-up transformers. All generators in the system are presented by a sixth-order model with exciter and governor. Conventional PSS has been included in generator 3 excitation system. An aggregated PV plant is connected to the grid at bus 6 in Area 1. Aggregation of collector system can be done by the National Renewable Energy Laboratory equivalencing method [14]. The MVA rating of the PV generator is assumed to be 25% of the exporting power of Area 1. There are two load buses in the system: Load 1 consists of 1767 MW and 100 MVAr, whereas Load 2 consists of 967 MW and 100 MVAr. System loads are considered as constant power P load. All system parameters are taken from [21].

In this study, controller location is fixed at PV, which means that the input matrix B is invariant. Thus, the value of joint controllability/observability measure depends on the output matrix

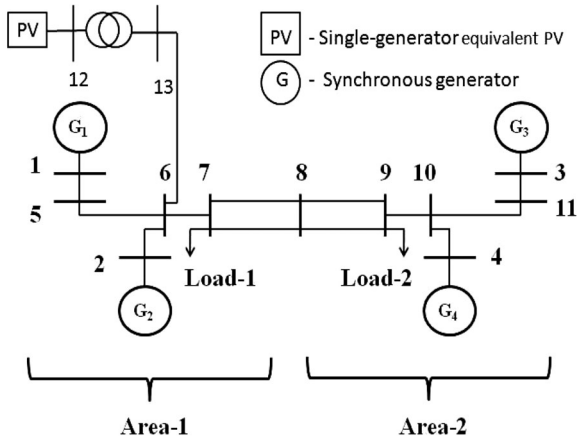

Fig. 7. Single-line diagram of a two-area test system.

C. As such, wide-area signal with maximal observability of target mode has been adopted as the input (feedback) signal of the POD. In this case, comparative strength of line power and current has been considered for input signal selection. The wide-area signal with maximal observability to the target (interarea) mode is power flow between *buses 9 and 10*. The step by step controller design procedure is presented next.

B. Controller Design Procedure

Design of POD for a PV plant includes the following steps:

Step 1: Linearize the two-area system around a chosen operating point.

Step 2: Conduct modal analysis to the linear system to get the eigenvalues, frequencies, and damping ratios corresponding to EM modes and identify the modes to be damped.

Step 3: Evaluate the comparative strength of the candidate signals to the given EM mode by modal controllability/observability [31].

Step 4: Form a state-space model of the system with time delays (first-order Padé approximation).

Step 5: Form a volume of probable system operating conditions and obtain the uncertainty gain matrix for a neighborhood (Ω) of a system operating point by using the following expression:

$$\tilde{\phi}(t) = [A_i(\gamma + \Delta\gamma) - A_i(\gamma)]$$

and $\phi(t)$ is obtained as

$$\phi(t) = \frac{1}{\sqrt{\alpha}}\tilde{\phi}(t).$$

Obtain α by numerical method to satisfy$\|\phi\|^2 \leq 1$.

Step 6: Check to see if there exists a feasible controller for α, i.e., if there exists a scalar τ such that there is a feasible solution for the coupled Riccati equations in Appendix B.

Step 7: If we obtain a feasible controller in the step earlier, enlarge Ω, i.e., increase the operating region, or if we

TABLE I
EM MODES OF OPEN-LOOP SYSTEM WITH AND WITHOUT PV

EM mode index	Mode type	Eigenvalues (with PV)	% ζ	Eigenvalues (without PV)	% ζ
1	inter-area	-0.06±j3.32	1.9	-0.12±j3.25	3.8
2	local	-0.49±j6.24	7.8	-0.49±j6.30	7.8
3	local	-0.49±j6.23	7.9	-0.50±j6.13	8.0

TABLE II
SENSITIVITY OF EM MODES TO THE DIFFERENT STATE WEIGHTS

No.	State weights $[\delta_1,\omega_1,\delta_2,\omega_2,\delta_3,\omega_3,\delta_4,\omega_4]$	Mode 1 % ζ	Mode 2 % ζ	Mode 3 % ζ
1	[0.1,0.1,0.1,0.1,0.1,0.1,0.1,0.1]	4.86	8.60	8.55
2	[1,1,1,1,1,1,1,1]	4.89	8.60	8.55
3	[1,1,1,1,0.1,0.1,0.1,0.1]	5.19	8.50	8.45
4	[0.1,0.1,0.1,0.1,1,1,1,1]	6.17	8.63	8.30
5	[1,1,1,1,2,2,2,2]	6.14	8.65	8.72

arrived at the largest possible operating region, then perform the optimal search for τ to get the infimum of V_τ. If there is no feasible solution for the coupled Riccati equations, go to *Step 5* and reduce the operating region.

Step 8: The obtained controller order is equal to the order of the system, which is difficult to handle for high-order systems. Therefore, the controller order is reduced by using the *balanced truncation* method, available in *Robust Control Toolbox* [32].

The term $x^T(t)Rx(t)$ in the cost function J in (11) represents the norm squared value of the nominal system output and $u^T(t)Gu(t)$ represents the design parameter affecting the controller gain. The initial guess for control parameter G is set to 10^{-4}. The weighting matrix R is constructed as a diagonal matrix, where nonzero weights are assigned to the states most participating to the mode and zero weights are assigned to other states. The values of R have been determined by trial and error. Furthermore, D_2 has been chosen according to the design criterion $D_2\ D_2^T > 0$ [11].

V. NUMERICAL RESULTS

A. Closed-Loop System Performance

A POD at a PV plant is designed for a two-area system, which is shown in Fig. 7. Some modifications have been made in the system to integrate the PV generator in Area 1. The modal analysis results of the system with and without the PV generator are shown in Table I. From Table I, it can be seen that the integration of PV at Area 1 reduces the damping ratio ζ of the interarea mode from 3.8% to 1.9%, resulting in longer time for oscillation to decay.

Table II shows the damping of EM modes with the full-order minimax LQG POD at PV for different state weights. From the table, it can be seen that the designed controller improves the interarea mode damping significantly (1.9% to 4.8% and more) for the selected state weights, resulting in quick decay of interarea oscillation. From Table II, it can be seen that for state weights $[0.1\quad 0.1\quad 0.1\quad 0.1\quad 1\quad 1\quad 1\quad 1]$, the designed controller

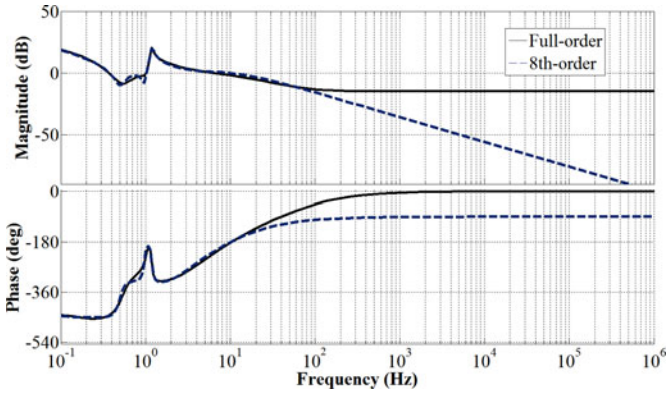

Fig. 8. Bode plot for controller approximation.

TABLE III
EM MODES OF A CLOSED-LOOP SYSTEM WITH THE REDUCED-ORDER (EIGHTH-ORDER) MINIMAX LQG POD

EM mode index	Mode type	Eigenvalues	% ζ
1	inter-area	-0.1942±j3.175	6.11
2	local	-0.5482±j6.25	8.60
3	local	-0.5299±j6.31	8.30

provides the best damping performance to the interarea mode. Hence, the designed controller with these state weights has been considered in this section for further analysis. It is also noticeable from the table that the damping ratios of the local modes are slightly increased by the integration of POD at PV.

Since the order of the designed minimax controller is equal to the plant order (the 64th order), the controller is too complex for practical implementation. Thus, simpler design without losing effectiveness was sought. Bode diagram approximation available at *Robust Control Toolbox* in MATLAB [32] is used to evaluate the effectiveness of the full- and reduced-order controller for the frequency of interest. Fig. 8 shows the Bode diagram approximation for the controller order reduction. It can be seen from the figure that the eighth-order controller is nearly indistinguishable compared to the full-order controller in the frequency up to 2 Hz, which includes all EM modes.

Table III shows the damping of the EM modes with the reduced-order (the eighth order) controller. From the table, it can be noticed that the eighth-order damping controller satisfactorily meets the damping requirement of the interarea mode for the full-power network. The damping ratios of the local modes are almost unaffected with the integration of the reduced-order damping controller at the PV generator.

Fig. 9 shows the open-loop and closed-loop system frequency response. It can be seen from the figure that there is higher overshoot in the magnitude response in the open-loop system. On the contrary, a closed-loop system magnitude response shows lower overshoot, resulting higher damping ratio to the interarea mode.

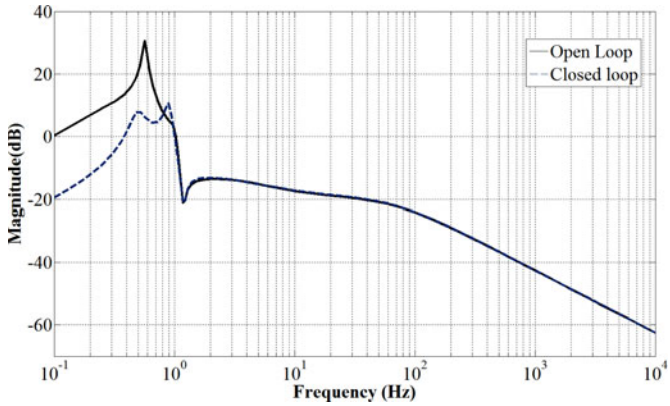

Fig. 9. Frequency response plot of the open-loop and closed-loop system.

TABLE IV
OPERATING CONDITIONS FOR A TWO-AREA TEST SYSTEM

Operating condition	Changed system topologies from base case
OC.1	Load: ZIP load (2734 MW); Output of G1 and G2 are 625 MW;
OC.2	Load: P load (2767 MW); Tie line power flow: 400 MW from Area 2 to 1;
OC.3	Load: P+I (2734 MW) [33]; Tie line Power flow: 300 MW from Area 2 to 1;
OC.4	Load: P (2784 MW); Output of G4 is 625 MW; Tie line power flow 450 MW;
OC.5	Load: Z (2935 MW); Output of G3 and G4 are 836 MW and 500 MW, respectively.

B. Evaluation of Controller Performance

The minimax LQG controller has been designed for a particular system operating condition (referred as nominal condition) by considering model uncertainty to the neighborhood of the operating condition.

Now, the performance of the designed controller is assessed for several operating conditions by considering different load characteristics as compared to a classical POD controller (lead/lag), since the change of load characteristics is quite common and has a significant effect on small signal stability, voltage stability, and transient stability [33], [34]. Table IV lists the different operating conditions for the assessment of minimax LQG and classical controller performance. There is always a possibility that the operating conditions other than these might be encountered in practice; but, these operating conditions in the table are identified as the probable ones. In the table, ZIP represents polynomial load, and I, P, and Z represent constant current, power, and impedance loads, respectively. Fig. 10 illustrates the percentage of damping for the open-loop and closed-loop system with minimax LQG and classical control under different operating conditions. From the figure, it can be seen that the proposed minimax LQG controller provides adequate damping (near 6% damping) to the interarea mode, not only for the nominal condition but also for different operating conditions. The damping of interarea mode for different operating conditions is in the close vicinity of that for the nominal condition (for which the controller is designed): 6.07%, 5.88%, 5.93%, 5.98%, and 6.03% for operating conditions 1 to 5, respectively. Fig. 10 also depicts that the classical controller has failed to provide adequate damping to the interarea mode for different operation conditions.

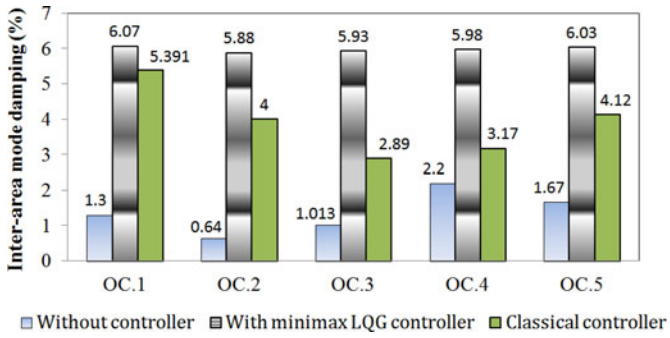

Fig. 10. Damping of interarea mode under different operating conditions.

TABLE V
DAMPING OF INTERAREA MODE FOR TIE-LINE OUTAGES

Controller type	Operating condition	Eigenvalues	% ζ	Freq. (Hz)
Minimax LQG	Pre-fault	-0.1942 ±j3.175	6.11	0.505
	Post-fault (outage: 7-8)	-0.1855 ±j3.190	5.81	0.507
	Post-fault (outage: 9-8)	-0.18450 ±j3.310	5.57	0.52
Classical	Pre-fault	-0.2025 ±j3.2873	6.2	0.523
	Post-fault (outage: 7-8)	-0.0976 ±j2.5421	3.83	0.40
	Post-fault (outage: 9-8)	-0.0788 ±j2.548	3.09	0.41

TABLE VI
DAMPING OF INTERAREA MODE FOR VARIOUS TIME DELAYS

Controller type	Time delays (ms)	120	150	180	200
Minimax LQG	Eigenvalues	-0.186 ±j3.11	-0.180 ±j3.12	-0.177 ±j3.11	-0.166 ±j3.10
	% ζ	5.96	5.76	5.69	5.36
	Freq.(Hz)	0.50	0.496	0.495	0.493
Classical	Eigenvalues	-0.181 ±j3.34	-0.172 ±j3.34	-0.154 ±j3.34	-0.146 ±j3.34
	% ζ	5.41	5.13	4.45	4.31
	Freq.(Hz)	0.53	0.53	0.53	0.53

It is evident from the obtained results that the proposed controller maintains robust damping performance under probable operating conditions compared to the classical POD at PV. The performance of the proposed controller as compared to the classical controller is further assessed for the severe faults (tie-line outages) and different time delays. Tables V and VI demonstrate the performance of the damping controllers for the outage of tie-lines and different time delays. It is clear from the results of Tables V and VI that the designed minimax LQG controller provides adequate damping to the interarea mode even during the severe fault conditions and different signal transmission delays. From the tables, it is evident that the classical POD at PV has failed to maintain adequate damping performance during the severe fault conditions and different time delays.

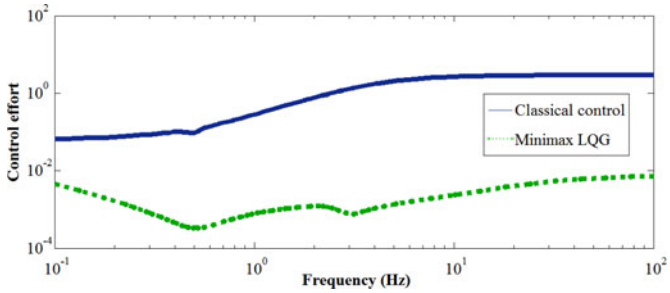

Fig. 11. Control effort of POD at PV.

TABLE VII
ROBUSTNESS ASSESSMENT RESULTS WITH AND WITHOUT POD

System configuration	μ-upper bounds
Without POD at PV (open loop)	1.2106
With minimax LQG POD at PV (closed loop)	0.845

Fig. 11 shows the control effort of POD at PV for classical and minimax LQG controller design. From the figure, it can be seen that classical control has higher gain in the frequency range of interest (0.2–0.8 Hz) compared to the minimax LQG control. This leads us to argue that the classical controller needs higher control energy than the minimax LQG controller for making near to similar improvement in the close-loop system damping.

C. Robustness Evaluation

Table VII shows the robust stability assessment results for the test system without and with the minimax LQG POD controller for a given range of parameter uncertainties. From the table, it can be seen that the open-loop system is not robustly stable with the given uncertainty range, as it shows μ-upper bound greater than 1(1.2106). The designed minimax LQG controller at PV is able to stabilize the system over the range of the given uncertainty as the μ-upper bound is less than 1(0.845).

As the simulation results in the earlier section depicted that the performance of the classical POD at PV is not adequate for different system operating conditions and requires higher control effort to get the similar control performance as compared to the proposed minimax LQG POD, thereby, the robustness evaluation of the system with this type has not been considered.

D. Validation by Nonlinear Simulation

A nonlinear simulation has been performed over a period of 25 s to further demonstrate the performance of the proposed controller in the presence of nonlinearties. Interarea oscillation is initiated by a self-clearing three-phase fault at bus 8 of the system at 1.00 s and cleared at 1.10 s. Fig. 12 shows the power flow response in the tie-line connecting buses 7–8. It can be seen from the figure that the oscillation in the power flow is settled within 10–12 s with the proposed controller.

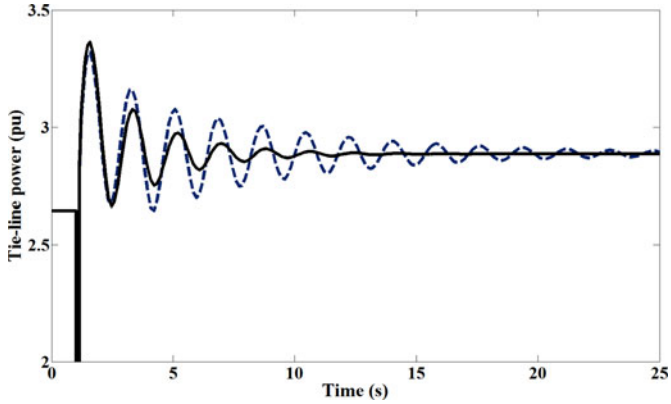

Fig. 12. Power flow response time-domain simulation (solid: with controller, dashed: without controller).

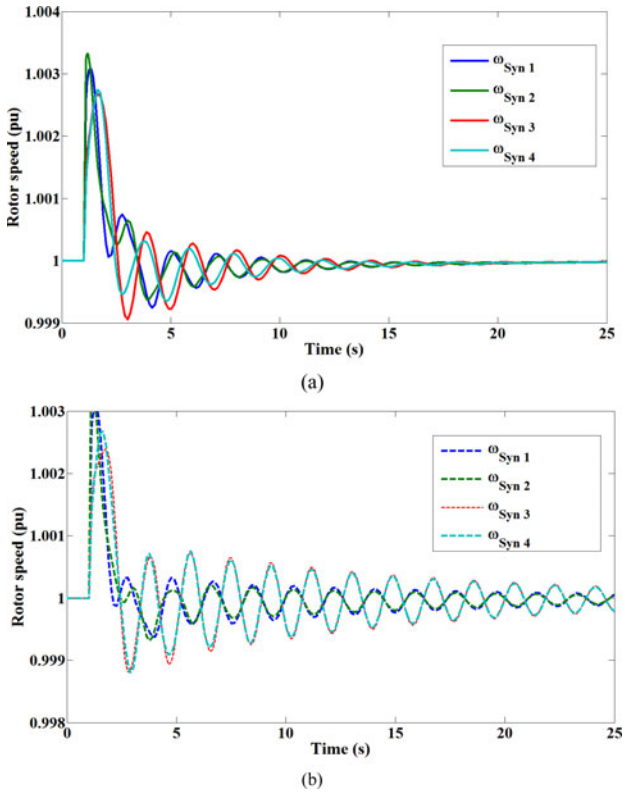

Fig. 13. Machine speeds time-domain simulation: (a) with controller, (b) without controller.

The results in Fig. 13 show the speed of machines with and without controller. It can be seen that the rotor speed oscillations damped out in 12–15 s. A 10–20 s settling time is adopted by many utilities in their system design and operational guidelines [35]. It is evident from the obtained results that the oscillations are settled within desired time.

Fig. 14 shows the dynamic response of voltage modes following the fault at bus 8. From the figure, it is clear that the proposed controller has no adverse effect on voltage modes of the system.

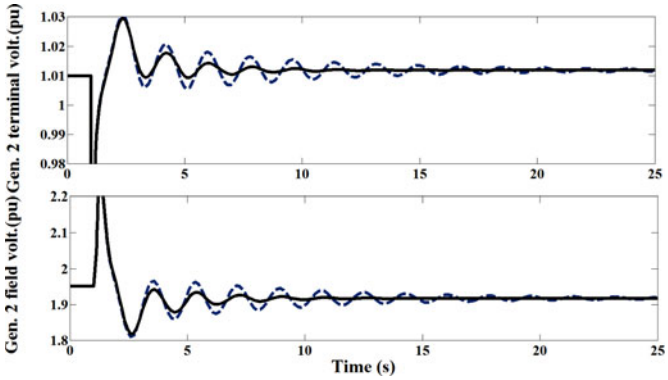

Fig. 14. Dynamic response of power system following fault at bus 8 (solid: with controller, dashed: without controller).

VI. Conclusion

This paper has demonstrated the possibility of using a wide-area measurement-based damping controller at a PV plant to effectively damp out the interarea oscillation resulting in a interconnected power grid. A systematic approach of designing POD based on the minimax LQG technique is described here. Possible signal latency of dedicated communication channel is taken into account for the controller design.

A reduced-order model of the designed controller has been tested under different operating conditions and time delays to verify its performance for interarea oscillation damping. From the simulation results, it is found that the proposed controller works satisfactorily under different operating conditions, including severe fault conditions. It is also found from the simulation studies that the damping of the target mode reduces with the increase in signal transmission delay. However, damping of the target mode is still above the acceptable limit of the utility for higher signal transmission delays. The effectiveness of the proposed method is also compared with the classical controller and found to be superior to the conventional one. The robustness is tested through computation of a s.s.v. and found that the designed minimax LQG-based POD is robust enough to keep the system stable over the range of uncertainties. It is worthwhile to note that the designed controller does not have any adverse effect on other modes of the system.

Appendix A
Power System Model

A. Synchronous Generator Model

$$\dot{\delta} = \omega_s(\omega - 1) \tag{A1}$$

$$\dot{\omega} = (P_m - P_e - D(\omega - 1))/M \tag{A2}$$

$$\dot{e}'_q = \left(-f_s(e'_q) - \left(x_d - x'_d - \frac{T''_{do}}{T'_{do}}\frac{x''_d}{x'_d}(x_d - x'_d)\right) i_d + \left(1 - \frac{T_{AA}}{T'_{do}}\right) v_f\right)/T'_{do} \tag{A3}$$

$$\dot{e}'_d = \left(-e'_d + \left(x_q - x'_q - \frac{T''_{qo}}{T'_{qo}}\frac{x''_q}{x'_q}(x_q - x'_q)\right) i_q\right) \Big/ T'_{qo} \tag{A4}$$

$$\dot{e}''_q = \left(-e''_q + e'_q - \left(x'_d - x''_d + \frac{T''_{do}}{T'_{do}}\frac{x''_d}{x'_d}(x_d - x'_d)\right) i_d + \frac{T_{AA}}{T'_{do}} v_f\right)\Big/ T''_{do} \tag{A5}$$

$$\dot{e}''_d = \left(-e''_d + e'_d + \left(x'_q - x''_q + \frac{T''_{qo}}{T'_{qo}}\frac{x''_q}{x'_q}(x_q - x'_q)\right) i_q\right) \Big/ T''_{qo}. \tag{A6}$$

The algebraic constraints associated with a synchronous generator model can be expressed as

$$\begin{cases} 0 = v_q + r_a i_q - e''_q + (x''_d - x_l) i_d \\ 0 = v_d + r_a i_d - e''_d - (x''_q - x_l) i_q. \end{cases}$$

In the model, δ is the rotor angle, ω is the rotor speed, e'_q is the quadrature-axis transient voltage, e'_d is the direct-axis transient voltage, e''_q is the quadrature-axis subtransient voltage, and e''_d is the direct-axis sub transient voltage. The definitions of the parameters in these equations can be found in [21] and will not be repeated here.

B. Exciter and PSS Model

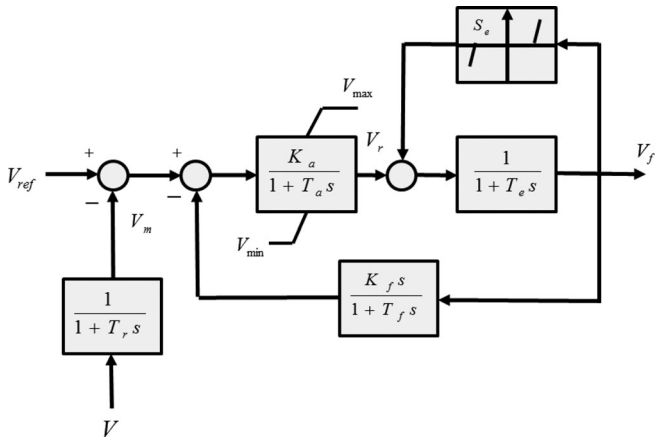

Fig. 15. IEEE type-I exciter system.

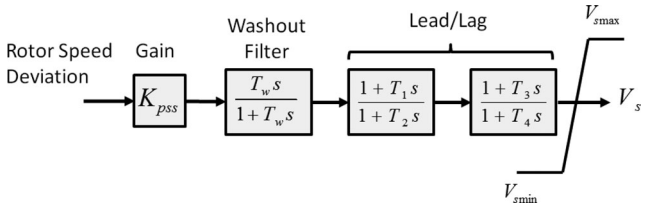

Fig. 16. Typical PSS model.

APPENDIX B
MINIMAX LQG CONTROL

The uncertainty input can be expressed as

$$\xi = \tilde{\phi}\tilde{C}_1\Delta x \tag{B1}$$

where $\tilde{\phi}$ is a uncertainty gain matrix. The matrix $\tilde{C}_1$ is chosen as an identity matrix. A scaling parameter α is chosen such that it satisfies the following constraints:

$$\|\phi\|^2 \leq 1,\ \|\xi\|^2 \leq \|\zeta\|^2$$

Now, $\phi = \tilde{\phi}/\sqrt{\alpha}$ and $C_1 = \sqrt{\alpha}\tilde{C}_1$.

The cost function J associated with minimax LQG satisfies

$$\sup_{\|\xi\|^2 \leq \|\zeta\|^2} J(u^*) \leq \inf_{\tau} V_\tau$$

where V_τ is an optimal value of risk sensitive control;

$$V_\tau = \frac{1}{2}tr\Big[Y_\infty R_\tau + \Big(Y_\infty C_2^T + B_2 D_2^T\Big)\Big(D_2 D_2^T\Big)^{-1} \times \Big(C_2 Y_\infty + D_2 B_2^T\Big) \times X_\infty\Big(I - \frac{1}{\tau}Y_\infty X_\infty\Big)^{-1}\Big]. \tag{B2}$$

Here, τ is a free parameter and the matrices X_∞ and Y_∞ are the solution to the following pair of parameter-dependent algebraic Riccati equations:

$$\Big(A - B_2 D_2^T\Big(D_2 D_2^T\Big)^{-1} C_2\Big)Y_\infty + Y_\infty\Big(A - B_2 D_2^T \times \Big(D_2 D_2^T\Big)^{-1} C_2\Big)^T - Y_\infty\Big(C_2^T (D_2 D_2^T\Big)^{-1} C_2 - \frac{1}{\tau}R_\tau\Big)Y_\infty + B_2\Big(I - D_2^T\Big(D_2 D_2^T\Big)^{-1} D_2\Big)B_2^T = 0 \tag{B3}$$

and

$$X_\infty\Big(A - B_1 G_\tau^{-1}\gamma_\tau^T\Big) + \Big(A - B_1 G_\tau^{-1}\gamma_\tau^T\Big)^T X_\infty + \Big(R_\tau - \gamma_\tau G_\tau^{-1}\gamma_\tau^T\Big) - X_\infty\Big(B_1 G_\tau^{-1} B_1^T - \frac{1}{\tau}B_2 B_2^T\Big)X_\infty = 0. \tag{B4}$$

Constraints to be satisfied: $Y_\infty > 0, X_\infty > 0$, the spectral radius of the matrix

$X_\infty Y_\infty$ is $\rho(X_\infty Y_\infty) < \tau, R_\tau - \gamma_\tau^T G_\tau^{-1}\gamma_\tau \geq 0, R_\tau = R + \tau C_1^T C_1, G_\tau = G + \tau D_1^T D_1$, and $\gamma_\tau = \tau C_1^T D_1$.

To obtain the minimax LQG controller, the parameter $\tau > 0$ is chosen to minimize V_τ. This involves solving the Riccati equations (B3) and (B4) for different values of τ and finding the value which gives the smallestV_τ.

ACKNOWLEDGMENT

The first author would like to thank Dr. M. Jahangir Hossain, from Griffith University, Nathan, Qld., Australia, for the interesting discussion about the minimax LQG scheme. The authors would like to thank all of the anonymous reviewers for their valuable suggestions that led them to conduct additional research and establish deeper understanding.

REFERENCES

[1] Photon Int. (Apr. 2011). *The Solar Power Magazine*, [Online]. Available: http://www.photon-magazine.com

[2] S. Achilles, A. Schramm, and J. Bebic, "Transmission system performance analysis for high penetration photovoltaics," Nat. Renewable Energy Laboratory, Golden, CO, Tech. Rep., NREL/SR-581-42300, Feb. 2008.

[3] Y. T. Tan, "Impact of power system with a large penetration of photovoltaic generation," Ph.D. dissertation, Inst. of Sci. and Technol., The Univ. of Manchester, Manchester, U.K., 2004.

[4] W. Du, H. F. Wang, and L.-Y. Xiao, "Power system small-signal stability as affected by grid-connected photovoltaic generation," *Eur. Trans. Electr. Power*, vol. 21, no. 5, pp. 688–703, Jul. 2011.

[5] R. Shah, N. Mithulananthan, A. Sode-Yome, and K. Y. Lee, "Impact of large-scale PV penetration on power system oscillatory stability," in *Proc. IEEE Power Energy Soc. General Meeting*, Minneapolis, MN, Jul. 25–29, 2010, pp. 1–7.

[6] J. H. R. Enslin, "Dynamic reactive power and energy storage for integrating intermittent renewable energy," in *Proc. IEEE Power Energy Soc. General Meeting*, Minneapolis, MN, Jul. 25–29, 2010, pp. 1–4.

[7] R. Shah, N. Mithulananthan, and K. Y. Lee, "Contribution of PV systems with ultracapacitor energy storage on inter-area oscillation," in *Proc. IEEE Power Energy Soc. General Meeting*, Detroit, MI, Jul. 24–28, 2011, pp. 1–8.

[8] R. Shah, N. Mithulananthan, and R. C. Bansal, "Damping performance analysis of battery energy storage, ultracapacitor and shunt capacitor with large-scale PV plants," *Appl. Energy Spec. Issue Smart Grid*, vol. 96, pp. 235–244, Aug. 2012.

[9] M.-G. Yoon, V. A. Ugrinovskii, and M. Pszezel, "Gain-scheduling of minimax optimal state-feedback controllers for uncertain LPV systems," *IEEE Trans. Autom. Control*, vol. 52, no. 2, pp. 549–557, Feb. 2007.

[10] A. Almutairi, "Enhancement of power system stability using wide area measurement system based damping controller," Ph.D. dissertation, School of Electr. and Electron. Eng., The Univ. of Manchester, Manchester, U.K., 2010.

[11] I. R. Petersen, V. A. Ugrinnovskii, and A. V. Savkin, *Robust Control Design Using H∞ Methods*. London, U.K.: Springer, 2000.

[12] M. J. Hossain, H. R. Pota, V. A. Ugrinovski, and R. A. Ramos, "Simultaneous STATCOM and pitch angle control for improved LVRT capability of fixed-speed wind turbines," *IEEE Trans. Sustainable Energy*, vol. 1, no. 3, pp. 142–151, Oct. 2010.

[13] *WECC Guide for Representation of Photovoltaic Systems in Large-Scale Load Flow Simulations*, WECC Renewable Energy Modeling Task Force Report, Aug. 2010.

[14] *Standard Report for Variable Generation*, NERC Special Report, Atlanta, GA, Feb. 2010.

[15] M. G. Villalva, J. R. Gazoli, and E. R. Filho, "Comprehensive approach to modeling and simulation of photovoltaic arrays," *IEEE Trans. Power Electron.*, vol. 24, no. 5, pp. 1198–1208, May 2009.

[16] F. Ferandez-Bernel, L. Rouco, P. Centeno, M. Gonzalez, and M. Alonso, "Modelling of photovoltaic plants for power system dynamic studies," in *Proc. IEEE Int. Conf. Power System Manage. Control*, Apr. 2002, pp. 341–346.

[17] K. Clark, N. W. Miller, and R. Walling, *Modeling of GE Solar Photovoltaic Plants for Grid Studies*. General Electrical International, Inc., Schenectady, NY, 2010.

[18] S.-Y. Ruan, G.-J. Li, B.-T. Ooi, and Y.-Z. Sun, "Power system damping from real and reactive power modulations of voltage source converter station," *IET Gener. Transm. Distrib.*, vol. 2, no. 3, pp. 311–320, 2008.

[19] A. Dysko, W. E. Leithead, and J. O'Reilly, "Enhanced power system stability by coordinated PSS design," *IEEE Trans. Power Systems*, vol. 25, no. 1, pp. 903–915, Feb. 2010.

[20] D. Dotta, A. Silva, and I. Decker, "Wide-area measurements-based two-level control design considering signal transmission delay," *IEEE Trans. Power Systems*, vol. 24, no. 1, pp. 208–216, Feb. 2009.
[21] P. Kundur, *Power System Stability and Control*. New York: McGraw-Hill, 1994.
[22] IEEE Working Group on Computer Modelling of Excitation Systems, "Excitation system models for power system stability studies," *IEEE Trans. Power App. Syst.*, vol. PAS-100, no. 2, pp. 494–509, Feb. 1981.
[23] W. Yao, Q. H. Wu, J. Y. Wen, and S. J. Cheng, "Delay-dependent stability analysis of the power system with a wide-area damping controller embedded," *IEEE Trans. Power Syst.*, vol. 26, no. 1, pp. 233–240, Feb. 2011.
[24] L. Philipp, A. Mahmood, and B. Philipp, "An improved refinable rational approximation to the ideal time delays," *IEEE Trans. Circuit Syst.*, vol. 46, no. 5, pp. 637–640, May 1999.
[25] H. Wu, K. S. Tsakalis, and G. T. Heydt, "Evaluation of time delays effects to wide-area power system stabilizer design," *IEEE Trans. Power Syst.*, vol. 19, no. 4, pp. 1935–1941, Nov. 2004.
[26] K. M. Son and J. K. Park, "On the robust LQG control of TCSC for damping power system oscillations," *IEEE Trans. Power Syst.*, vol. 15, no. 4, pp. 1306–1312, Nov. 2000.
[27] A. C. Zolostas, B. Chaudhuri, I. M. Jaimoukha, and P. Korba, "A study on LQG/LTR control for damping inter-area oscillations in power systems," *IEEE Trans. Control Syst. Technol.*, vol. 15, no. 1, pp. 151–160, Jan. 2007.
[28] Z. Pan and T. Basar, "Model simplification and optimal control of stochastic singularity perturbed systems under exponential quadratic cost," *SIAM J. Control Optimization*, vol. 34, no. 5, pp. 1734–1766, 1996.
[29] M. Djukanovic, M. Khammash, and V. Vittal, "Application of structured singular value theory for robust stability and control analysis in multimachine power systems. I. framework development," *IEEE Trans. Power Syst.*, vol. 13, no. 4, pp. 1311–1316, Nov. 1998.
[30] H. Nguyen-Duc, L. Dessaint, and A. Okou, "Power system robust stability analysis using structured singular value theory and modal reduction method," in *Proc. IEEE Power Energy Soc. General Meeting*, Calgary, AB, Canada, Jul. 26–30, 2009, pp. 1–8.
[31] A. Heniche and I. Kamwa, "Control loops selection to damp inter-area oscillations of electrical networks," *IEEE Trans. Power Syst.*, vol. 17, no. 2, pp. 378–384, May 2002.
[32] G. Balas, R. Chiang, A. Packard, and M. Safonov Robust Control Toolbox for Matlab, 2005.
[33] I. Kamwa, G. Gorndin, and Y. Trudel, "IEEE PSS2B versus PSS4B: The limits of performance of modern power system stabilizers," *IEEE Trans. Power Syst.*, vol. 20, no. 2, pp. 903–915, May 2005.
[34] N. Mithulananthan and C. A. Canizares, "HOPF bifurcations and critical mode damping of power systems for different static load models," in *Proc. IEEE Power Energy Soc. General Meeting*, Denver, CO, Jun. 6–10, 2004, pp. 1877–1882.
[35] J. Paserba, Analysis and Control of Power System Oscillation: CIGRE Special Publication 38.01.07, vol. Technical Brochure 111, 1996.

Rakibuzzaman Shah (S'10) received the B.Sc. Eng. degree in electrical and electronic engineering from Khulna University of Engineering & Technology, Khulna, Bangladesh, and the M.Eng. degree from the Asian Institute of Technology, Bangkok, Thailand, in 2005 and 2009, respectively. He is currently working toward the Ph.D. degree at the University of Queensland, Brisbane, Qld., Australia.

He has served as a Lecturer at the Chittagong University of Engineering & Technology, Bangladesh, for one and half years. His main research interests include power system stability, energy security, power system interconnection, and renewable energy technology.

Nadarajah Mithulananthan (SM'10) received the Ph.D. degree in electrical and computer engineering from the University of Waterloo, Waterloo, ON, Canada, in 2002.

He was an Electrical Engineer at the Generation Planning Branch of Ceylon Electricity Board, Sri Lanka, and as a Researcher at Chulalongkorn University, Bangkok, Thailand. He is currently a Senior Lecturer at the University of Queensland, Brisbane, Qld., Australia. He has also served as an Associate Professor at the Asian Institute of Technology, Bangkok, Thailand. His main research interests include voltage stability and oscillation studies on practical power systems, application of FACTS controller, and renewable energy technology.

Kwang Y. Lee (F'01) received the B.S. degree in electrical engineering from Seoul National University, Seoul, Korea, in 1964, the M.S. degree in electrical engineering from North Dakota State University, Fargo, in 1968, and the Ph.D. degree in system science from Michigan State University, East Lansing, in 1971.

He has been on the faculties of Michigan State University, Oregon State University, University of Houston, the Pennsylvania State University, and Baylor University, Waco, TX, where he is currently a Professor and the Chair of electrical and computer engineering and the Director of Power and Energy Systems Laboratory. His research interests include power systems control, operation and planning, and intelligent systems applications to power plants and power systems control.

Dr. Lee served as an Editor of IEEE TRANSACTIONS ON ENERGY CONVERSION, and an Associate Editor of IEEE TRANSACTIONS ON NEURAL NETWORK.